NANO LETTERS

pubs.acs.org/NanoLett

Letter

Dynamic Color Tuning with Electrochemically Actuated TiO_2 Metasurfaces

Janna Eaves-Rathert, Elena Kovalik, Chibuzor Fabian Ugwu, Bridget R. Rogers, Cary L. Pint, and Jason G. Valentine*

Cite This: *Nano Lett.* 2022, 22, 1626−1632

Read Online

ACCESS | Metrics & More | Article Recommendations | Supporting Information

ABSTRACT: Dynamic tuning of metamaterials is a critical step toward advanced functionality and improved bandwidth. In the visible spectrum, full spectral color tuning is inhibited by the large absorption that accompanies index changes, particularly at blue wavelengths. Here, we show that the electrochemical lithiation of anatase TiO_2 to $Li_{0.5}TiO_2$ (LTO) results in an index change of 0.65 at 649 nm with absorption coefficient less than 0.1 at blue wavelengths, making this material well-suited for dynamic visible color tuning. Dynamic tunability of TiO_2 is leveraged in a Fabry−Perot cavity and a gap plasmon metasurface. In the Fabry−Perot configuration, the device exhibits a shift in reflectance of over 100 nm when subjected to only 2 V bias while the gap plasmon metasurface achieves enhanced switching speed. The dynamic range, speed, and cyclability indicate that the TiO_2/LTO system is competitive with established actuators like WO_3, with the additional advantage of reduced absorption at high frequencies.

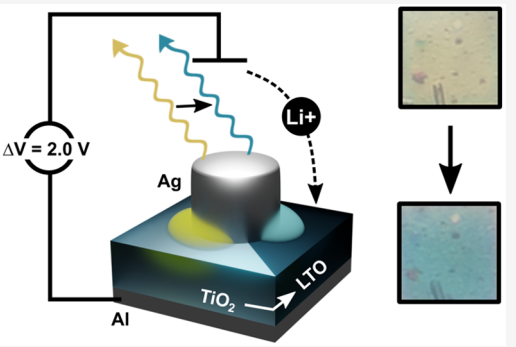

KEYWORDS: *Nanophotonics, metamaterials, electrochromism, structural color, gap plasmon, optical properties, lithium ion*

INTRODUCTION

Color can be categorized as pigmentary or structural, and while pigmentary colors eliminate certain wavelengths of light due to absorption at energies dictated by electronic transitions, structural color is generated from physical geometry. Since structural color does not directly rely on absorption, materials with ultralow loss can be harnessed to build vibrant colors through interference, diffraction, or scattering. Active control over structural color is a burgeoning field of interest with applications in areas such as anticounterfeiting, consumer electronics, thermoregulation, and camouflage.[1,2] Furthermore, decoupling the electromagnetic response from intrinsic material properties allows for access to numerous modalities for dynamic color tuning. Approaches to modulation can be separated into two categories: (1) mechanical reconfiguration of the geometry and arrangement of scatterers; (2) manipulation of the optical properties of the scatterer or its environment for a resulting change in resonance frequency.[2] Although there are a variety of paths to achieve modulation, electrochemistry is the only method that belongs to both categories as it can provide large changes in geometry[3] as well as modulation of the carrier concentration[4,5] made possible by ionic diffusion and charge compensation, therein overcoming Debye screening effects.[4]

Considering the vast arsenal of materials available for optoelectrochemical tuning, it has been particularly challenging to find a continuously tunable material with high index and transparency throughout the visible spectrum, particularly in the blue region. To date, only a few materials systems have been leveraged for electrochemical tuning of metamaterials, but they either experience high losses in the visible (i.e., Si, metals) or have limited dynamic range (i.e., polymers, WO_3). Titanium dioxide (TiO_2) is a popular material for photonics due to its high index and low absorption coefficient, and while the electrochromic properties of TiO_2 nanoparticles are well-known,[6−9] there remain ample opportunities to further harness this phenomenon for structural color tuning. In metasurfaces, the transition metal oxide has found a multitude of applications including planar metalenses,[10−12] perfect reflectors,[13] subtractive color filters,[14] and aberration correction.[15] There has been a demonstration of a tunable TiO_2 metasurface using ion implantation in which the structural color of an array was fully damped,[16] but many applications require functionality beyond amplitude modulation.

Meanwhile, in the electrochemistry community, TiO_2 is a reliable anode material for lithium ion batteries, known for excellent cycle life and minimal volume expansion.[17−21] The

Received: November 29, 2021
Revised: February 2, 2022
Published: February 9, 2022

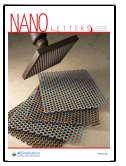

https://doi.org/10.1021/acs.nanolett.1c04613
Nano Lett. 2022, 22, 1626−1632

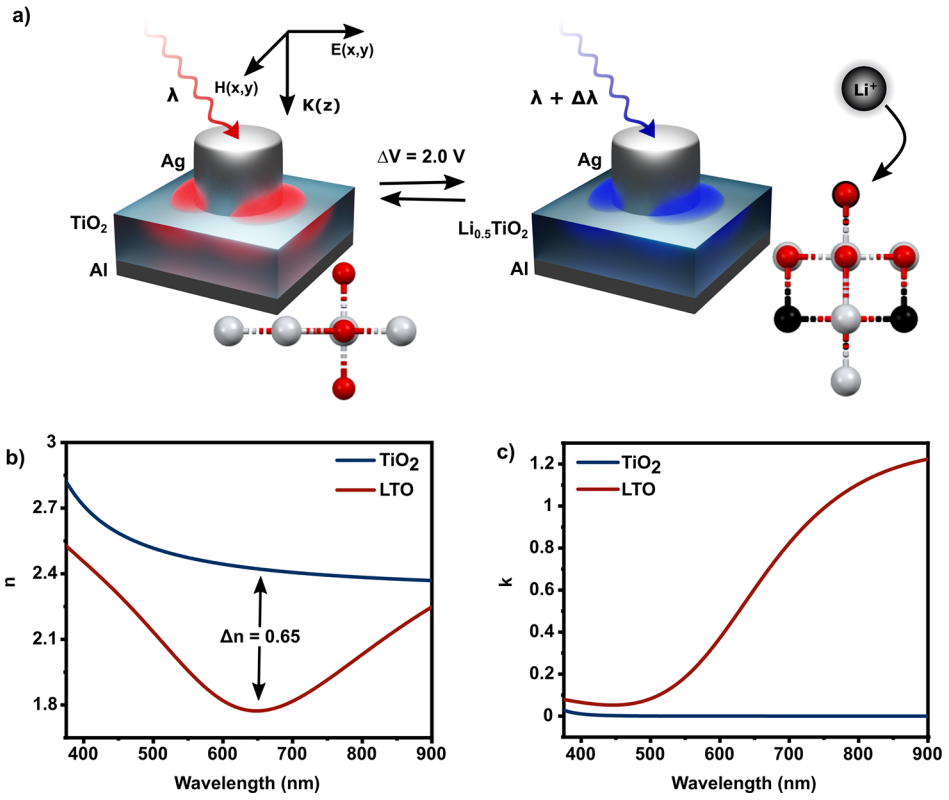

Figure 1. Concept of electrochemical modulation using the TiO_2/LTO materials system. (a) Depiction of modulation mechanism, showing the change in resonant wavelength of gap plasmon structures caused by lithium ion intercalation in TiO_2. Crystal structures for anatase TiO_2[36] and orthorhombic LTO[37] were visualized using Mercury.[38] (b) Change in refractive index and (c) absorption coefficient derived from ellipsometry measurements.

reversible reaction is well studied: $TiO_2 + xLi^+ + xe^- \rightarrow Li_xTiO_2$, where x is the mole fraction of Li.[22] Upon Li^+ intercalation up to $x = 0.5$, the tetragonal symmetry of anatase ($I4_1/amd$) is broken, forming orthorhombic $Li_{0.5}TiO_2$ ($Imma$) which is accompanied by ~5% volume change.[22−24] At $0.05 < x < 0.5$, TiO_2 and $Li_{0.5}TiO_2$ coexist in a two-phase system, resulting in a constant potential during charge and discharge. Insertion of additional lithium is possible for nanostructures and thin films at low current densities but results in reduced Li^+ ion mobility.[17,22,25,26] To our knowledge at the time of writing, the dielectric function of electrochemically lithiated $Li_{0.5}TiO_2$ (henceforth referred to as LTO) has never been experimentally measured.

Here, we critically evaluate the TiO_2/LTO system as an electrochemical tuning agent for active metamaterials and demonstrate its efficacy for modulation of nanophotonic structures. In contrast to previous studies of electrochromism in TiO_2, the incorporation of resonant nanostructures harnesses both real and imaginary parts of the complex dielectric function to produce vibrant structural color spanning the visible spectrum. We first demonstrate a simple Fabry−Perot nanocavity, which reflects frequencies of light that satisfy the resonance criteria between two reflective surfaces.[27] In a second demonstration, TiO_2 serves as the dielectric in a metal−insulator−metal (MIM) type gap plasmon metasurface, where enhanced electromagnetic fields[28,29] lead to smaller mode volumes and accelerated switching speeds. This work illustrates how nanophotonic design in conjunction with electrochemically activated media allows flexible control over spectral response.

RESULTS AND DISCUSSION

In this work, the dielectric properties of TiO_2 are transformed by applying a voltage between the device and a counter electrode, causing lithium ions to reversibly intercalate into the TiO_2. When incorporated into nanophotonic devices, the resulting phase transformation is expected to shift the resonant frequency as shown in Figure 1a. To predict the breadth of optical modulation in the proposed configurations, we first experimentally determined the dielectric function of TiO_2 and its lithiated counterpart using spectroscopic ellipsometry. TiO_x films were deposited on silicon wafers via RF magnetron sputtering and subsequently annealed in air at 400 °C to yield anatase TiO_2,[30−35] confirmed through Raman spectroscopy (Figure S1). Spectroscopic ellipsometry was used to determine the refractive index (n) and absorption coefficient (k), and the results are presented in Figure 1b and Figure 1c, respectively. A refractive index of 2.42 at 650 nm is consistent with other reports of annealed TiO_2.[10,11,35] Raw ellipsometry data are included in Figure S2, along with fit parameters used for modeling (Table 1 in Supporting Information). The absorption coefficient is negligible throughout the visible spectrum, though it increases at lower wavelengths as photon energy approaches the band edge.

Significant modification of the refractive index and extinction coefficient was achieved through electrochemical lithiation of anatase TiO_2. Orthorhombic Li_xTiO_2 (LTO) was formed through ambient temperature galvanostatic discharge of anatase in 1 M $LiClO_4$ electrolyte to a capacity of 168 mAh·g^{-1}, corresponding to $x = 0.5$ (Figure S3), at which point the sample was rinsed in dry acetonitrile and transferred directly

https://doi.org/10.1021/acs.nanolett.1c04613
Nano Lett. 2022, 22, 1626−1632

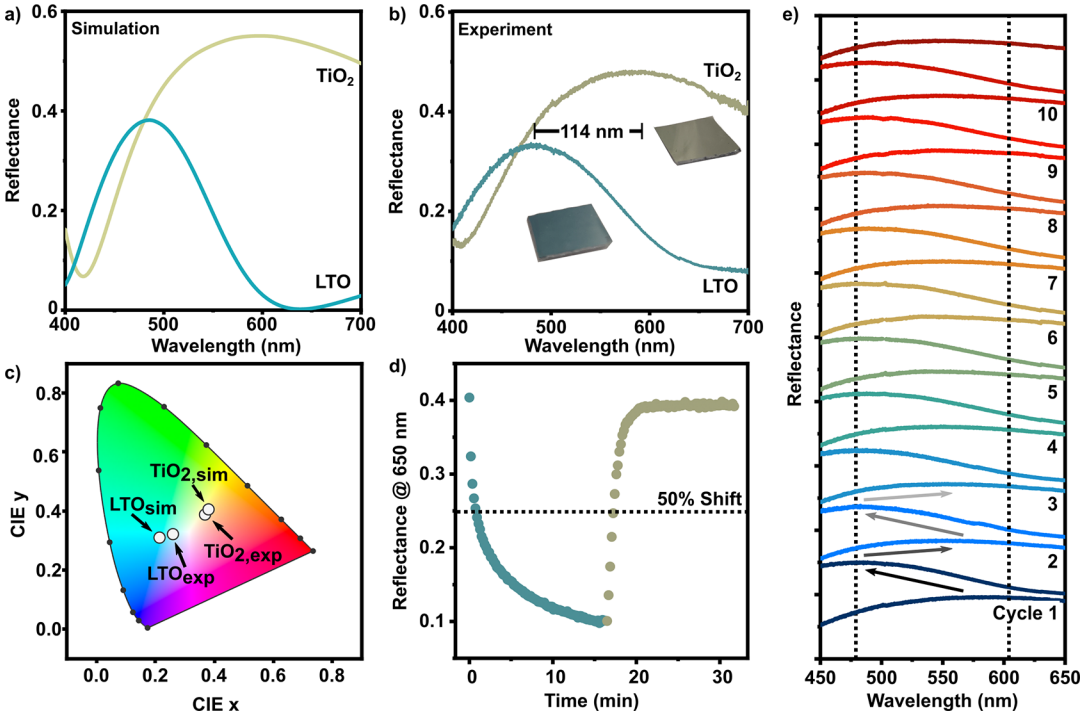

Figure 2. Performance of Fabry–Perot nanocavities in optical cell. (a) Theoretical reflectance spectra for a cavity comprised of TiO_2 versus LTO film, simulated using measured optical constants. Line colors represent color calculated from spectra. (b) Experimental reflectance spectra for pristine film and lithiated film after galvanostatic discharge to −2 V. Line colors represent color calculated from spectra. (c) CIE 1931 chromaticity map with points representing experimentally measured and simulated color of TiO_2 and LTO films. (d) Speed of color change determined by plotting the magnitude of reflectance at 650 nm acquired every 10 s during potentiostatic hold at −2 V. (e) Reversibility of spectral shift over 10 cycles.

into a homemade air-free ellipsometry compartment inside a glovebox. After application of the fit parameters detailed in Table 2 in Supporting Information, the result is a dip in refractive index with a minimum of 1.77 at 650 nm, generating a maximum shift of $\Delta n = 0.65$ at 649 nm ($\Delta\varepsilon_1 = 3.15$ at 707 nm), likely related to the interband transitions of localized electrons previously identified at 700 nm (1.77 eV) by Wagemaker et al.[39] Nearing the band gap, absorption remains very low due to the Moss–Burstein effect,[40] suggesting the possibility of high-efficiency, tunable metasurfaces across the entire visible spectrum. For reference, the absorption coefficient of Li_xTiO_2 with $x = 0.5$ is 50% less than that of the popular transition metal oxide, Li_xWO_3, with $x > 0.38$ at blue wavelengths.[41,42] The resulting values of n and k are in agreement with optical properties extracted from DFT calculations, as shown in Figure S4. The chemical underpinnings of the observed optical transitions were verified using X-ray photoelectron spectroscopy (XPS), revealing that approximately 41% of the Ti atoms are in a reduced state after lithiation (Figure S5). More information about ellipsometry, DFT, and XPS measurements is available in the Supporting Information.

With the aim of demonstrating the dynamic tuning capabilities of anatase TiO_2 in simplest form, basic Fabry–Perot nanocavities were fabricated through the deposition of 100 nm TiO_x onto a titanium metal backplane, which was subsequently annealed at 400 °C in air to form anatase TiO_2. Reflections off the TiO_2–air interface and the metal backplane interact in a weakly resonant cavity that appears gold in the pristine state. Finite element frequency-domain (FD) simulations executed using the experimentally determined dielectric functions for TiO_2 predicted broadband reflection of visible wavelengths greater than 500 nm in the pristine state, with a local minimum around 410 nm due to destructive interference in the cavity, as shown in Figure 2a. By replacing TiO_2 with the lower-index LTO and increasing thickness by 5% to represent volume expansion associated with the phase transformation,[25,43] new resonance conditions dictated reflection of blue-green wavelengths, peaking around 490 nm. The minimal thickness expansion contributes a small red shift of ∼7 nm, as illustrated in Figure S12. In practice, spectral reflections in the pristine state agreed closely with simulations, despite being slightly damped by interfacial losses in the optical cell (see Figure S7) and finite roughness of the TiO_2 surface. The experimental results shown in Figure 2b agree with simulations, therein confirming the dielectric function for LTO derived from ellipsometry measurements. For the first discharge, the full extent of tunability was achieved by slowly discharging at a constant current of 1 $\mu A/cm^2$, generating a 114 nm blue shift as the optical thickness of the cavity is decreased. Notably, the maximum peak intensity of the lithiated film experienced a reduction of 38.7%, in line with predictions, supporting the selection of the TiO_2/LTO system for highly efficient tuning across the visible spectrum. The chromaticity was calculated from the reflectance spectra and mapped in the CIE 1931 color space in Figure 2c. More information about color identification and mapping is provided in the Supporting Information. The color purity, represented as the radial component of chromaticity, is slightly lower than that predicted through simulation, likely due to the nuances of nanostructured anatase when operated at high rates. For very small particles, high surface energy may prohibit phase

https://doi.org/10.1021/acs.nanolett.1c04613
Nano Lett. 2022, 22, 1626–1632

coexistence, causing individual grains to transform instantaneously rather than proceeding through the film as a uniform phase front.[26] This behavior results in an effective mixing of TiO_2 and LTO properties, broadening the resonance and reducing the color purity. Such phenomena can be mitigated by slowing the reaction or by using thicker films with bulk properties.

The greatest rate of change in reflectance spectra is observed in the early stages of intercalation (Figure 2d). Immediately after application of voltage, a buildup of capacitance at the interface gives way to the solid solution regime, followed by rapid nucleation of the LTO phase. Given the small nucleation energy barrier, the phase boundary motion is fast compared with lithium self-diffusion; thus the reaction rate slows as the system transitions into a diffusion-limited regime.[26] Accordingly, a large initial shift in peak wavelength after the first 30 s is succeeded by more and more subtle adjustments over the total holding period of 15 min. For insertion, 50% of the total reflection change is achieved within the first 50 s. Upon reversal, the 50% benchmark is achieved in just over 40 s. Such asymmetry has been evaluated in other works[22,44] and is theoretically attributed to a higher energy barrier across the phase boundary during insertion.[22]

Although significant spectral shifts are possible in short times, the device is cycled to the extent of its capability using potentiostatic holds at −2 V (insertion) and 0 V (extraction) for up to 15 min each (Figure 2e). In doing so, we find that the device demonstrates full optical reversibility over the first 10 cycles, following an initial first cycle loss of only 5.5% the total reflected power. In the fourth and tenth cycles, the peak-to-peak shifts in reflectance were 62.9 and 61.2 nm, respectively, indicating negligible additional loss after the first few cycles. It should be noted that the external bias of only 2 V is an order of magnitude less than the voltages applied to devices based on state-of-the-art phase change materials.[45−47] Furthermore, the lithiated and delithiated states were highly stable after 20 min under open circuit conditions, suggesting the device is nonvolatile and exhibits bistability (Figure S8).

To better understand the limits of speed and cyclability for this material system, we measured the cycle life and diffusion coefficient of lithium in the sputtered TiO_2 thin films. The capacity retention for a 20 nm anatase film on an aluminum backplane cycled in a coin cell versus LFP is shown in Figure 3a. After 400 cycles of galvanostatic charge and discharge at 3 $\mu A/cm^2$ (30 min per cycle) the lithium capacity remains stable, despite initial capacity loss associated with solid electrolyte interphase formation and volume expansion. Following this, the capacity is constant over the duration of cycling with a slight increase attributed to fine adjustments in microstructure that allows accommodation of additional lithium ions. This observation is consistent with the previously discussed optoelectrochemical cycling studies of Fabry−Perot nanocavities. The excellent electrochemical cyclability of anatase thin films is expected to translate into dynamic photonic devices which maintain full modulation depth over many switching cycles.

Switching speed is a critical parameter for most optoelectronic devices. In electrochemical systems, the speed will primarily depend on film thickness and the intrinsic diffusion coefficient. The diffusion coefficient was derived from the transient current response of a planar electrode to an instantaneous potential step,[48−50] and the results are shown in Figure 3b. When stepped from the open circuit voltage to

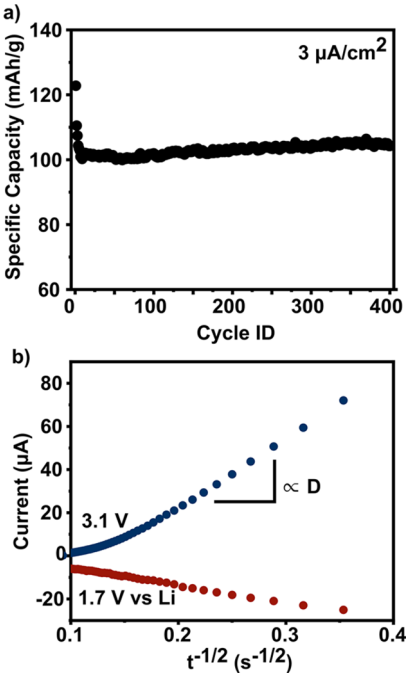

Figure 3. Electrochemical characterization of TiO_2 films. (a) Cycle life of 20 nm TiO_2 films on Al backplane cycled at 3 $\mu A/cm^2$ in coin cells versus LFP cathode. (b) Results of potential step experiment for 100 nm TiO_2 films on Ti in three-electrode flooded cell with platinum counter electrode and $Ag/AgNO_3$ reference electrode. The slope of the curve is proportional to the diffusion coefficient.

−1.5 V vs $Ag/AgNO_3$ (1.67 V vs Li/Li^+), the slope of current versus $t^{-1/2}$ is predominantly linear, curving slightly with increasing time to indicate a minor dependence of diffusion characteristics on lithium content.[22,51] Taking the average linear slope (R^2 = 0.997), the diffusion coefficient for lithium insertion was calculated as 9.78×10^{-12} cm^2/s. On the reverse step, a much higher current at early times is associated with a greater diffusion coefficient of 9.31×10^{-11} cm^2/s. These values agree with other measurements of lithium diffusion in anatase TiO_2[22,25,51] and establish an upper boundary on speed through the characteristic diffusion time, $\tau_d = l^2/D$, where l is the film thickness. For a 100 nm film, the characteristic diffusion time is 10.2 s for insertion and 1.07 s for extraction, though speed can be dramatically improved by reducing thickness; for a 20 nm film, the characteristic diffusion time is 0.409 s for insertion and 0.043 s for extraction. As this represents the ideal (upper bound) for speed, the slightly longer measured switching speed (Figure 2) is attributed to sources of impedance in the optoelectrochemical cell, particularly non-negligible ionic resistance through the separator and electrolyte.

In order to realize faster actuation times, the same material system was incorporated into a gap plasmon metasurface. For the metal−insulator−metal configuration with patterned nanopillars atop a thin dielectric layer, strong absorption in the gap is enabled by the resonant behavior of excited gap surface plasmons.[52,53] 20 nm thick TiO_2 films were chosen as the dielectric layer between patterned silver nanopillars and an aluminum backplane, simultaneously optimizing coupling and reducing the diffusion path length of Li^+ ions to enhance reaction speed. The final unit cell design is depicted in Figure 4a. For all tests, the period of the patterned layer remains a constant 250 nm and the pillar height is 40 nm. As pillar

https://doi.org/10.1021/acs.nanolett.1c04613
Nano Lett. 2022, 22, 1626−1632

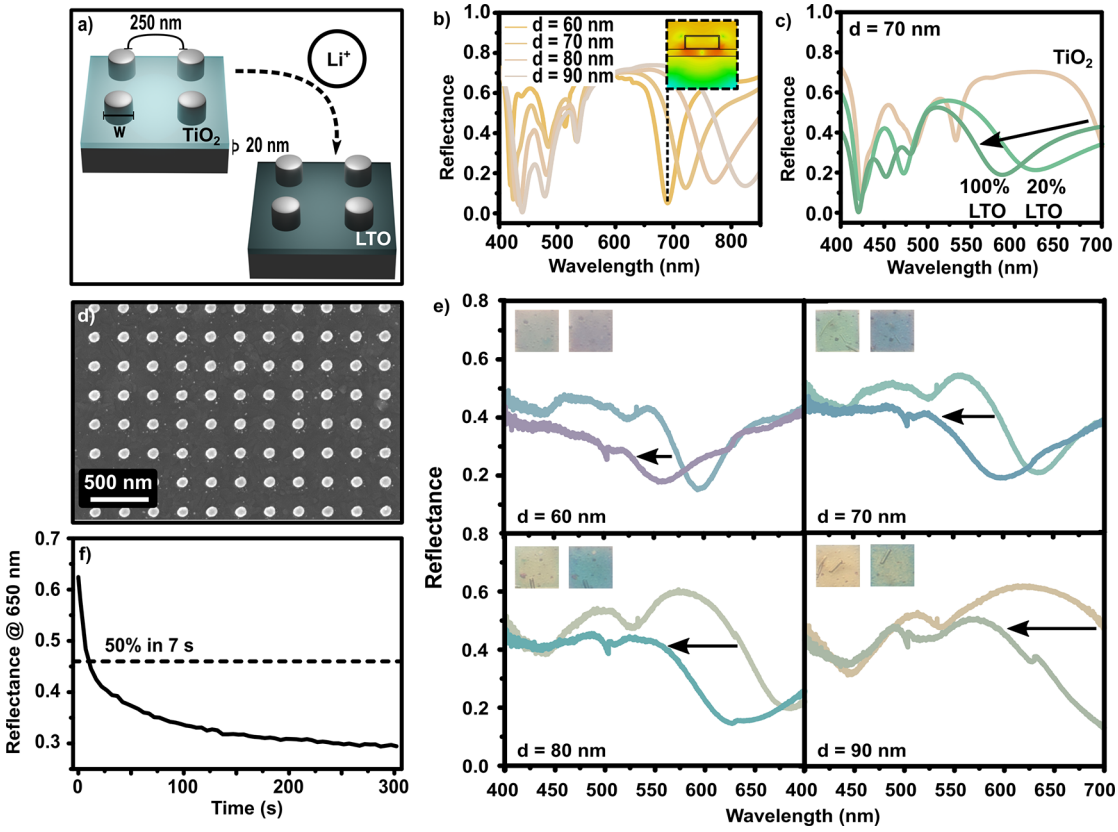

Figure 4. Performance of gap plasmon device in optical cell. In all plots, line colors represent color calculated from spectra. (a) Schematic of device unit cell before and after lithium intercalation. (b) Simulated reflectance spectra for varying pillar diameter from 60−90 nm. Inset shows electric field distribution at the frequency corresponding to the peak minimum. (c) Simulated reflectance spectra for 70 nm diameter pillars with LTO content ranging from 0% to 100%. (d) SEM image of metasurface acquired at 5 kV, magnification = 100K×, working distance = 5.0 mm. (e) Experimentally measured reflectance spectra showing shifts for four different pillar diameters after galvanostatic lithiation. Insets are photographs of the arrays in each state. (f) Speed of reflectance change at 650 nm.

diameter varies from 60 to 90 nm, FD simulations predict a red shift in the reflectance minimum (Figure 4b), as the resonance condition for counter-propagating gap surface plasmon polaritons dictates destructive interference at increasingly long wavelengths.[53] As shown in Figure 4b, inset, the electric field is concentrated in the gap between pillar and backplane at the frequency of minimum reflectance. The reflected color is thereby tuned from gold to brown with increasing pillar diameter. The positions of local minima at shorter wavelengths are not strongly dependent on resonator width due to near-field coupling between neighboring surface plasmon polaritons. Considering the case of 70 nm pillar diameter, changing LTO content was simulated as a uniform phase front propagating along the depth of the film in Figure 4c. As the film is transformed from anatase TiO_2 to 100% LTO, the reflectance minimum experiences a significant blue shift of 135 nm, changing the expected color from gold to green. An SEM image of the fabricated metasurface is included in Figure 4d. In experimental demonstrations (Figure 4e), the positions of the gap plasmon resonances are consistent with expectations for the lithiated state, but the pristine spectra are slightly blue-shifted, potentially stemming from diffusion of silver into the TiO_2 thin film during e-beam evaporation.[54,55] The silver can diffuse beneath the resist layer and renucleate at the surface, forming constellations of silver nanoislands around the larger pillars (Figure S9). Due to the sensitivity of plasmon polaritons to the environment at the metal−dielectric interface, this introduces an offset in the initial state of the device. Accordingly, the spectral shifts in reflectance minima are 59, 39, and 37 nm for the 80, 70, and 60 nm diameter pillars, respectively. Though the minima for the 90 nm pillars are cut off by the detector window, there is a significant blue shift in the peak edge measuring 108 nm. Figure 4e shows that the most significant shift occurs in the first few seconds with diminishing returns at longer time scales. When considering the change in reflectance over time at 650 nm, 50% change is realized in 7 s, a time scale that compares favorably with similar devices constructed using Li_xWO_3.[4,41] Though the transition is still slower than the measured diffusion coefficient would suggest, the speed of ion transport is likely limited by elements of device construction and can be optimized using different cell components and geometries. These results lay the foundation for applications of the TiO_2/LTO material system in tunable nanophotonic devices for the visible spectrum. Additional data and results for a similar device using aluminum nanopillars are illustrated in Supporting Information Figures S10 and S11.

CONCLUSIONS

As shown here, TiO_2 is an attractive material for dynamic tuning of photonic devices in the visible spectrum, leveraging a reversible electrochemically controlled phase transformation at biases less than 2 V. This results in a change in refractive index of 0.65 while maintaining a small absorption coefficient at blue wavelengths. These properties, combined with measured

https://doi.org/10.1021/acs.nanolett.1c04613
Nano Lett. 2022, 22, 1626−1632

diffusion coefficients on the order of 10^{-11} cm/s and stable cycling of lithium at high rates, enable this material system as a suitable platform for active modulation. Employed in nanophotonic structures, this enables resonance tuning exceeding 100 nm. Employed as all-dielectric metasurfaces, this material system could open new doors in applications such as anticounterfeiting, holograms, or tunable aberration correction.

■ ASSOCIATED CONTENT

Supporting Information

The Supporting Information is available free of charge at https://pubs.acs.org/doi/10.1021/acs.nanolett.1c04613.

Experimental procedures as well as additional characterization results, including Raman spectroscopy, XPS, ellipsometry, cyclic voltammetry, electro-optical testing, and SEM of metasurfaces (PDF)

■ AUTHOR INFORMATION

Corresponding Author

Jason G. Valentine − *Department of Mechanical Engineering, Vanderbilt University, Nashville, Tennessee 37235, United States;* orcid.org/0000-0001-9943-7170; Email: jason.g.valentine@vanderbilt.edu

Authors

Janna Eaves-Rathert − *Department of Mechanical Engineering, Vanderbilt University, Nashville, Tennessee 37235, United States*

Elena Kovalik − *Interdisciplinary Materials Science Program, Vanderbilt University, Nashville, Tennessee 37235, United States*

Chibuzor Fabian Ugwu − *Department of Mechanical Engineering, Vanderbilt University, Nashville, Tennessee 37235, United States*

Bridget R. Rogers − *Department of Chemical and Biomolecular Engineering, Vanderbilt University, Nashville, Tennessee 37235, United States*

Cary L. Pint − *Department of Mechanical Engineering, Iowa State University, Ames, Iowa 50011, United States;* orcid.org/0000-0003-4700-0852

Complete contact information is available at: https://pubs.acs.org/10.1021/acs.nanolett.1c04613

Notes

The authors declare no competing financial interest.

■ ACKNOWLEDGMENTS

J.E.-R. acknowledges support from a NSF graduate fellowship under Grant 1445197, and J.G.V. acknowledges support from Northrop Grumman.

■ REFERENCES

(1) Jung, C.; Kim, G.; Jeong, M.; Jang, J.; Dong, Z.; Badloe, T.; Yang, J. K. W.; Rho, J. Metasurface-Driven Optically Variable Devices. *Chem. Rev.* **2021**, *121* (21), 13013−13050.

(2) Hail, C. U.; Michel, A. U.; Poulikakos, D.; Eghlidi, H. Optical Metasurfaces: Evolving from Passive to Adaptive. *Adv. Opt. Mater.* **2019**, *7* (14), 1801786.

(3) Wang, G.; Chen, X.; Liu, S.; Wong, C.; Chu, S. Mechanical Chameleon through Dynamic Real-Time Plasmonic Tuning. *ACS Nano* **2016**, *10*, 1788−1794.

(4) Li, Y.; van de Groep, J.; Talin, A. A.; Brongersma, M. L. Dynamic Tuning of Gap Plasmon Resonances Using a Solid-State Electrochromic Device. *Nano Lett.* **2019**, *19* (11), 7988−7995.

(5) Zanotto, S.; Blancato, A.; Buchheit, A.; Muñoz-Castro, M.; Wiemhöfer, H.-D.; Morichetti, F.; Melloni, A. Metasurface Reconfiguration through Lithium-Ion Intercalation in a Transition Metal Oxide. *Adv. Opt. Mater.* **2017**, *5* (2), 1600732.

(6) Patil, R. A.; Devan, R. S.; Liou, Y.; Ma, Y. R. Efficient Electrochromic Smart Windows of One-Dimensional Pure Brookite TiO2 Nanoneedles. *Sol. Energy Mater. Sol. Cells* **2016**, *147*, 240−245.

(7) Ghicov, A.; Tsuchiya, H.; Hahn, R.; MacAk, J. M.; Muñoz, A. G.; Schmuki, P. TiO2 Nanotubes: H+insertion and Strong Electrochromic Effects. *Electrochem. commun.* **2006**, *8* (4), 528−532.

(8) Chen, J. Z.; Ko, W. Y.; Yen, Y. C.; Chen, P. H.; Lin, K. J. Hydrothermally Processed TiO 2 Nanowire Electrodes with Antireflective and Electrochromic Properties. *ACS Nano* **2012**, *6* (8), 6633−6639.

(9) Dinh, N. N.; Oanh, N. T. T.; Long, P. D.; Bernard, M. C.; Hugot-Le Goff, A. Electrochromic Properties of TiO2 Anatase Thin Films Prepared by a Dipping Sol-Gel Method. *Thin Solid Films* **2003**, *423* (1), 70−76.

(10) Devlin, R. C.; Khorasaninejad, M.; Chen, W. T.; Oh, J.; Capasso, F. Broadband High-Efficiency Dielectric Metasurfaces for the Visible Spectrum. *Proc. Natl. Acad. Sci. U. S. A.* **2016**, *113* (38), 10473−10478.

(11) Khorasaninejad, M.; Chen, W. T.; Zhu, A. Y.; Oh, J.; Devlin, R. C.; Roques-Carmes, C.; Mishra, I.; Capasso, F. Visible Wavelength Planar Metalenses Based on Titanium Dioxide. *IEEE J. Sel. Top. Quantum Electron.* **2017**, *23* (3), 43−58.

(12) Khorasaninejad, M.; Chen, W. T.; Devlin, R. C.; Oh, J.; Zhu, A. Y.; Capasso, F. Metalenses at Visible Wavelengths: Diffraction-Limited Focusing and Subwavelength Resolution Imaging. *Science (80-.)* **2016**, *352* (6290), 1190−1194.

(13) Huang, Y.; Xu, H.; Lu, Y.; Chen, Y. All-Dielectric Metasurface for Achieving Perfect Reflection at Visible Wavelengths. *J. Phys. Chem. C* **2018**, *122*, 2990−2996.

(14) Koirala, I.; Lee, S.; Choi, D. Highly Transmissive Subtractive Color Filters Based on an All-Dielectric Metasurface Incorporating TiO2 Nanopillars. *Opt. Express* **2018**, *26* (14), 18320.

(15) Chen, W. T.; Zhu, A. Y.; Sanjeev, V.; Khorasaninejad, M.; Shi, Z.; Lee, E.; Capasso, F. A Broadband Achromatic Metalens for Focusing and Imaging in the Visible. *Nat. Nanotechnol.* **2018**, *13* (3), 220−226.

(16) Wu, Y.; Yang, W.; Fan, Y.; Song, Q.; Xiao, S. TiO2 Metasurfaces: From Visible Planar Photonics to Photochemistry. *Sci. Adv.* **2019**, *5* (11), No. eaax0939.

(17) Zakharova, G. S.; Jähne, C.; Popa, A.; Täschner, C.; Gemming, T.; Leonhardt, A.; Büchner, B.; Klingeler, R. Anatase Nanotubes as an Electrode Material for Lithium-Ion Batteries. *J. Phys. Chem. C* **2012**, *116* (15), 8714−8720.

(18) Lim, E.; Shim, H.; Fleischmann, S.; Presser, V. Fast and Stable Lithium-Ion Storage Kinetics of Anatase Titanium Dioxide/Carbon Onion Hybrid Electrodes. *J. Mater. Chem. A* **2018**, *6* (20), 9480−9488.

(19) Ortiz, G. F.; Hanzu, I.; Knauth, P.; Lavela, P.; Tirado, J. L.; Djenizian, T. TiO2 Nanotubes Manufactured by Anodization of Ti Thin Films for On-Chip Li-Ion 2D Microbatteries. *Electrochim. Acta* **2009**, *54* (17), 4262−4268.

(20) Xu, J.; Jia, C.; Cao, B.; Zhang, W. F. Electrochemical Properties of Anatase TiO2 Nanotubes as an Anode Material for Lithium-Ion Batteries. *Electrochim. Acta* **2007**, *52* (28), 8044−8047.

(21) Liu, Y.; Yang, Y. Recent Progress of TiO2-Based Anodes for Li Ion Batteries. *J. Nanomater.* **2016**, *2016*, 8123652.

(22) Wagemaker, M.; van de Krol, R.; Kentgens, A. P. M.; van Well, A. A.; Mulder, F. M. Two Phase Morphology Limits Lithium Diffusion in TiO 2 (Anatase): A 7 Li MAS NMR Study. *J. Am. Chem. Soc.* **2001**, *123* (46), 11454−11461.

(23) Cava, R. J.; Murphy, D. W.; Zahurak, S.; Santoro, A.; Roth, R. S. The Crystal Structures of the Lithium-Inserted Metal Oxides

Li0.5TiO2 Anatase, LiTi2O4 Spinel, and Li2Ti2O4. *J. Solid State Chem.* **1984**, *53* (1), 64−75.
(24) Nuspl, G.; Yoshizawa, K.; Yamabe, T. Lithium Intercalation in TiO2 Modifications. *J. Mater. Chem.* **1997**, *7* (12), 2529−2536.
(25) Wagemaker, M.; Borghols, W. J. H.; van Eck, E. R. H.; Kentgens, A. P. M.; Kearley, G. J.; Mulder, F. M. The Influence of Size on Phase Morphology and Li-Ion Mobility in Nanosized Lithiated Anatase TiO2. *Chem. - A Eur. J.* **2007**, *13* (7), 2023−2028.
(26) Shen, K.; Chen, H.; Klaver, F.; Mulder, F. M.; Wagemaker, M. Impact of Particle Size on the Non-Equilibrium Phase Transition of Lithium-Inserted Anatase TiO2. *Chem. Mater.* **2014**, *26* (4), 1608−1615.
(27) Atherton, P. D.; Reay, N. K.; Ring, J.; Hicks, T. R. Tunable Fabry-Perot Filters. *Opt. Eng.* **1981**, *20* (6), 69−76.
(28) Bozhevolnyi, S. I. Effective-Index Modeling of Channel Plasmon Polaritons. *Opt. Express* **2006**, *14* (20), 9467.
(29) Moreau, A.; Ciracì, C.; Mock, J. J.; Smith, D. R.; Hill, R. T.; Chilkoti, A.; Wang, Q.; Wiley, B. J. Controlled-Reflectance Surfaces with Film-Coupled Colloidal Nanoantennas. *Nature* **2012**, *492*, 86−89.
(30) Mathews, N. R.; Morales, E. R.; Cortés-Jacome, M. A.; Toledo Antonio, J. A. TiO2 Thin Films − Influence of Annealing Temperature on Structural, Optical and Photocatalytic Properties. *Sol. Energy* **2009**, *83* (9), 1499−1508.
(31) Horprathum, M.; Chindaudom, P.; Limsuwan, P. A Spectroscopic Ellipsometry Study of TiO2 Thin Films Prepared by dc Reactive Magnetron Sputtering: Annealing Temperature Effect. *Chin. Phys. Lett.* **2007**, *24* (6), 1505−1508.
(32) Pitna Laskova, B.; Kavan, L.; Zukalova, M.; Mocek, K.; Frank, O. In Situ Raman Spectroelectrochemistry as a Useful Tool for Detection of TiO2(Anatase) Impurities in TiO2(B) and TiO2-(Rutile). *Monatshefte fur Chemie* **2016**, *147* (5), 951−959.
(33) Frank, O.; Zukalova, M.; Laskova, B.; Kürti, J.; Koltai, J.; Kavan, L. Raman Spectra of Titanium Dioxide (Anatase, Rutile) with Identified Oxygen Isotopes (16, 17, 18). *Phys. Chem. Chem. Phys.* **2012**, *14* (42), 14567−14572.
(34) Niilisk, A.; Moppel, M.; Pärs, M.; Sildos, I.; Jantson, T.; Avarmaa, T.; Jaaniso, R.; Aarik, J. Structural Study of TiO2 Thin Films by Micro-Raman Spectroscopy. *Cent. Eur. J. Phys.* **2006**, *4* (1), 105−116.
(35) Eiamchai, P.; Chindaudom, P.; Pokaipisit, A.; Limsuwan, P. A Spectroscopic Ellipsometry Study of TiO2 Thin Films Prepared by Ion-Assisted Electron-Beam Evaporation. *Curr. Appl. Phys.* **2009**, *9* (3), 707−712.
(36) Wagemaker, M.; Kearley, G. J.; Van Well, A. A.; Mutka, H.; Mulder, F. M. Multiple Li Positions inside Oxygen Octahedra in Lithiated TiO2 Anatase. *J. Am. Chem. Soc.* **2003**, *125* (3), 840−848.
(37) Weirich, T. E.; Winterer, M.; Seifried, S.; Hahn, H.; Fuess, H. Rietveld Analysis of Electron Powder Diffraction Data from Nanocrystalline Anatase, TiO2. *Ultramicroscopy* **2000**, *81* (3−4), 263−270.
(38) Macrae, C. F.; Sovago, I.; Cottrell, S. J.; Galek, P. T. A.; McCabe, P.; Pidcock, E.; Platings, M.; Shields, G. P.; Stevens, J. S.; Towler, M.; Wood, P. A. Mercury 4.0: From Visualization to Analysis, Design and Prediction. *J. Appl. Crystallogr.* **2020**, *53* (1), 226−235.
(39) Wagemaker, M.; Lützenkirchen-Hecht, D.; Van Well, A. A.; Frahm, R. Atomic and Electronic Bulk versus Surface Structure: Lithium Intercalation in Anatase TiO2. *J. Phys. Chem. B* **2004**, *108* (33), 12456−12464.
(40) Van De Krol, R.; Goossens, A.; Meulenkamp, E. A. Electrical and Optical Properties of TiO2 in Accumulation and of Lithium Titanata Li0.5TiO2. *J. Appl. Phys.* **2001**, *90* (5), 2235−2242.
(41) Lee, Y.; Yun, J.; Seo, M.; Kim, S. J.; Oh, J.; Kang, C. M.; Sun, H. J.; Chung, T. D.; Lee, B. Full-Color-Tunable Nanophotonic Device Using Electrochromic Tungsten Trioxide Thin Film. *Nano Lett.* **2020**, *20* (8), 6084−6090.
(42) Wang, Z.; Wang, X.; Cong, S.; Chen, J.; Sun, H.; Chen, Z.; Song, G.; Geng, F.; Chen, Q.; Zhao, Z. Towards Full-Colour Tunability of Inorganic Electrochromic Devices Using Ultracompact Fabry-Perot Nanocavities. *Nat. Commun.* **2020**, *11* (1), 302.
(43) Zhu, J.; Feng, J.; Lu, L.; Zeng, K. In Situ Study of Topography, Phase and Volume Changes of Titanium Dioxide Anode in All-Solid-State Thin Film Lithium-Ion Battery by Biased Scanning Probe Microscopy. *J. Power Sources* **2012**, *197*, 224−230.
(44) van de Krol, R.; Goossens, A.; Schoonman, J. Spatial Extent of Lithium Intercalation in Anatase TiO 2. *J. Phys. Chem. B* **1999**, *103* (34), 7151−7159.
(45) Kim, Y.; Wu, P. C.; Sokhoyan, R.; Mauser, K.; Glaudell, R.; Kafaie Shirmanesh, G.; Atwater, H. A. Phase Modulation with Electrically Tunable Vanadium Dioxide Phase-Change Metasurfaces. *Nano Lett.* **2019**, *19* (6), 3961−3968.
(46) Gholipour, B.; Zhang, J.; MacDonald, K. F.; Hewak, D. W.; Zheludev, N. I. An All-Optical, Non-Volatile, Bidirectional, Phase-Change Meta-Switch. *Adv. Mater.* **2013**, *25* (22), 3050−3054.
(47) Hosseini, P.; Wright, C. D.; Bhaskaran, H. An Optoelectronic Framework Enabled by Low-Dimensional Phase-Change Films. *Nature* **2014**, *511* (7508), 206−211.
(48) Bard, A. J.; Faulkner, L. R. *Electrochemical Methods: Fundamentals and Applications*; Wiley, 2001.
(49) Kavan, L.; Grätzel, M.; Gilbert, S. E.; Klemenz, C.; Scheel, H. J. Electrochemical and Photoelectrochemical Investigation of Single-Crystal Anatase. *J. Am. Chem. Soc.* **1996**, *118* (28), 6716−6723.
(50) Lunell, S.; Stashans, A.; Ojamäe, L.; Lindström, H.; Hagfeldt, A. Li and Na Diffusion in TiO2 from Quantum Chemical Theory versus Electrochemical Experiment. *J. Am. Chem. Soc.* **1997**, *119* (31), 7374−7380.
(51) Moitzheim, S.; De Gendt, S.; Vereecken, P. M. Investigation of the Li-Ion Insertion Mechanism for Amorphous and Anatase TiO 2 Thin-Films. *J. Electrochem. Soc.* **2019**, *166* (2), A1−A9.
(52) Pors, A.; Bozhevolnyi, S. I. Gap Plasmon-Based Phase-Amplitude Metasurfaces: Material Constraints [Invited]. *Opt. Mater. Express* **2015**, *5* (11), 2448.
(53) Bozhevolnyi, S. I.; Søndergaard, T. General Properties of Slow-Plasmon Resonant Nanostructures: Nano-Antennas and Resonators. *Opt. Express* **2007**, *15* (17), 10869.
(54) Haque, S. M.; De, R.; Tripathi, S.; Sharma, R. K.; Polaki, S. R.; Rao, K. D. Plasmonic Effect of Diffused Ag Nanoparticles in EB Evaporated Ag/TiO2 Bilayer Thin Films and Role of Oxygen Pressure. *J. Alloys Compd.* **2020**, *849*, 156553.
(55) Zuo, J.; Rao, J.; Eggeler, G. Interface Reactions of Ag@TiO2 Nanocomposite Films. *Mater. Chem. Phys.* **2014**, *145* (1−2), 90−98.

https://doi.org/10.1021/acs.nanolett.1c04613
Nano Lett. 2022, 22, 1626−1632